Systematic combination of palladium facets and monolayer metal hydroxide nanosheets for promotion of ethanol oxidation reaction

Sho Kitano, Hiroya Motohashi, Mana Iwai, Koji Fushimi, Yoshitaka Aoki, Hiroki Habazaki**

*Sho Kitano: Division of Applied Chemistry, Faculty of Engineering, Hokkaido University, Sapporo, Hokkaido 060-8628, Japan

Hiroya Motohashi: Graduate School of Chemical Sciences and Engineering, Hokkaido University, Sapporo, Hokkaido 060-8628, Japan

Mana Iwai: Division of Applied Chemistry, Faculty of Engineering, Hokkaido University, Sapporo, Hokkaido 060-8628, Japan

Koji Fushimi: Division of Applied Chemistry, Faculty of Engineering, Hokkaido University, Sapporo, Hokkaido 060-8628, Japan

Yoshitaka Aoki: Division of Applied Chemistry, Faculty of Engineering, Hokkaido University, Sapporo, Hokkaido 060-8628, Japan

*Hiroki Habazaki: Division of Applied Chemistry, Faculty of Engineering, Hokkaido University, Sapporo, Hokkaido 060-8628, Japan

KEYWORDS: ethanol oxidation reaction, palladium, shape control, facet, nanosheet

ABSTRACT

The design of catalyst surfaces that exhibit high activities for ethanol oxidation reaction (EOR) is essential to achieving practical application of direct ethanol fuel cells. Composite catalysts of Pd nanoparticles and metal hydroxide are promising candidates for EOR; however, a guide of catalyst design, including appropriate valence states and interfacial structures between component materials, has not been identified. Herein, we synthesize composite electrocatalysts of cubic and octahedral Pd nanocrystals with well-defined facets and monolayer metal hydroxide nanosheets with an identical structure and different composition containing Ni, Fe and Mn, and systematically elucidate highly active interfacial sites between Pd and metal hydroxides for EOR. The valence states of Pd are oxidatively changed by nanosheets modification and the composite catalysts with higher oxidative states show higher EOR activities, probably due to stronger adsorption of ethanol molecules. Promotion of OH^- adsorption by hydroxide nanosheets also enhances the catalytic activities, and the improved activities are greater for (111) facet than for (100) facet of Pd whereas the (100) facet is superior for EOR to the (111) facet for the bare Pd nanocrystals. Our study suggests that combination of the Pd (111) facet and metal hydroxides is favorable for developing highly active electrocatalysts for EOR.

Introduction

The development of alternative energy sources to replace fossil fuels is an essential agenda for modern society. Fuel cells are prospective technologies to produce clean electricity because they convert chemical energy (fuel) into electrical energy with high efficiency and emit almost no pollutants[1]. Direct ethanol fuel cells (DEFCs) have been considered a promising candidate due to their high energy density, low toxicity, and convenient storage and transportation of liquid ethanol[2]. Commercially available Pt/C and Pt-based materials are commonly used in DEFCs as anode electrocatalysts for ethanol oxidation reaction (EOR) [3-5], but they are in a predicament of high cost and limited resources. Compared to Pt, Pd-based catalysts are regarded as alternatives to platinum for EOR, particularly in an alkaline environment, due to high intrinsic catalytic activities[6-8]. Therefore, improving the catalytic activity and stability of Pd-based catalysts is a challenging issue to meet the requirements of commercial applications and has emerged as a topic of recent hot debate.

Fabrication of composite structures with transition metal hydroxides or oxides such as $Ni(OH)_2$[9-10] and CuO[11-12] is one of the effective strategies to improve the catalytic performance of Pd-based catalysts. It has been reported that the introduction of metal hydroxides results in a synergistic interaction between Pd and metal hydroxides, which changes the electronic states of Pd and regulates the bonding between Pd and the reaction intermediates[11, 13-15]. Furthermore, the metal hydroxides can promote the supply of OH^- species from electrolytes due to a high affinity between the metal centers and the OH^- species, which accelerates dehydrogenation and oxidative removal of carbonaceous intermediates on the Pd surface[9]. Although several metal hydroxides achieved to improve catalytic activities of Pd nanoparticles for EOR, previous studies have not systematically investigated the effects of the kinds of metal hydroxide, structure of the contacting interface, and

facets of the materials on catalytic activities of composite catalysts, lacking effective design guide of highly active electrocatalysts.

Facet control is also an effective approach to achieve surface structure manipulation leading to the design of highly active catalysts[16-20]. Studies on Pd bulk single crystals have shown that the crystallographic orientations can have significant impacts on the various electrochemical reactions including EOR. The three basal planes (111), (100) and (110) are of fundamental interest since they are combined to form structurally high-index planes in single crystals[21]. From a practical viewpoint, Pd nanocrystals are preferable to Pd bulk crystals for employment as electrocatalysts. The basic nanofacets can be created on the surface of shape-controlled nanoparticles; for example, Pd cubes, octahedrons and rhombic dodecahedrons are enclosed predominantly by the (100), (111) and (110) nanofacets, respectively. Thus, a systematic investigation of the electrocatalytic activities of the Pd catalysts with controlled facets for EOR in alkaline media is highly demanded for development of highly efficient fuel cells. Based on the backgrounds, the combination of facet-controlled Pd nanocrystals and metal hydroxides will provide a design guide of highly active electrocatalysts for EOR. However, to the best of our knowledge, there is no report on the composite electrocatalysts of facet-controlled Pd nanocrystals and metal hydroxides for EOR.

In general, materials such as metal hydroxides with different compositions have different sizes, morphology and crystal structure, and these factors have complicated effects on catalytic properties. Since these factors change together when the kinds of metal hydroxide are changed, it is difficult to investigate the effects of metal hydroxides in composite catalysts systematically. Layered double hydroxide (LDH) is a layered compound that consists of metal hydroxide nanosheets containing various divalent and trivalent metal elements such as Ni^{2+}, Fe^{3+} and Mn^{3+} and water molecules and anions inserted between the layers[22-23]. The OH^- is preferentially

adsorbed on metal species at the edges of monolayer nanosheets exfoliated from LDH. The LDH has the same hydrotalcite crystal structure regardless of their various metal compositions, and the exfoliated monolayer nanosheets also have the same structure. In other words, exfoliated monolayer nanosheets have the same structure, but their chemical properties can be controlled by the metal composition. Therefore, the application of monolayer metal hydroxide nanosheets exfoliated from LDH to the shape-controlled Pd nanocrystals allows us to systematically investigate the composite effects on the catalytic performance for EOR.

In this study, we synthesize composite electrocatalysts of cubic and octahedral Pd nanocrystals and two kinds of monolayer metal hydroxide nanosheets exfoliated from LDHs containing Ni, Fe and Mn, and systematically investigate the effects of a combination of metal hydroxides with the (100) and (111) facets of Pd on catalytic performances of EOR to elucidate highly active interfacial sites between Pd and metal hydroxides (Scheme 1). Combination of metal hydroxide nanosheets improved catalytic performances of Pd nanocrystals by oxidative change in valence states of Pd and promotion of OH^- adsorption. We reveal that the metal hydroxide nanosheets have different effects on the facets of Pd and combination of the nanosheet containing Ni and Mn and Pd nanocrystals with the (111) facet is a promising way to enhance catalytic activities for EOR.

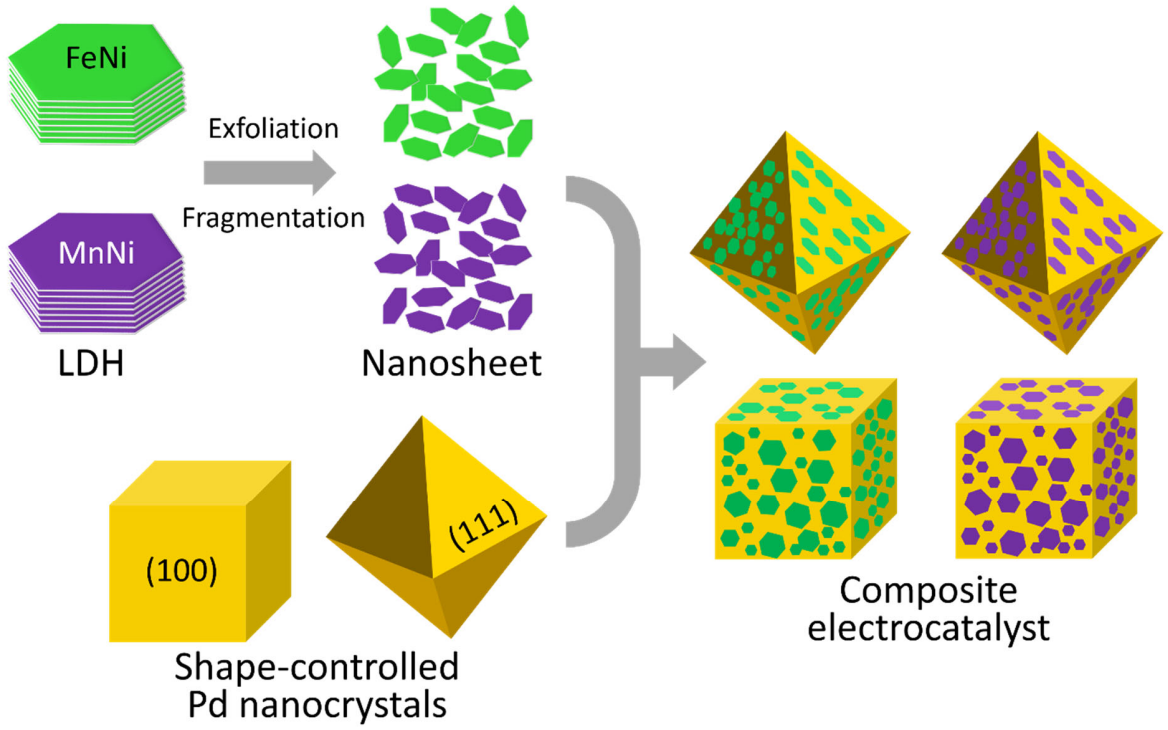

Scheme 1 Illustration of synthesis of the composite electrocatalysts of shape-controlled Pd nanocrystals and metal hydroxide nanosheets exfoliated from LDH.

Experimental

2.1 Synthesis of shape-controlled Pd nanoparticles

All the chemicals were of analytical grade and used without further purification.

Palladium (II) chloride ($PdCl_2$), palladium (II) sodium chloride (Na_2PdCl_4), potassium iodide (KI), cetyltrimethylammonium bromide (CTAB, Tokyo Chemical Industry Co., Ltd.)), cetyltrimethylammonium chloride (CTAC), L-ascorbic acid, citric acid and hydrochloric acid

(HCl) were obtained from Fujifilm Wako pure chemical corporation. Distilled water was used throughout the experiments.

The cubic and octahedral Pd nanoparticles were prepared by one-pot synthesis, as reported previously[19]. A 10 mmol dm^{-3} H_2PdCl_4 solution was prepared by dissolving 0.1773 g of $PdCl_2$ in 10 cm^3 of 0.2 mol dm^{-3} HCl solution and further diluting to 100 mL with doubly distilled water. In the synthesis of cubic Pd, a 5 cm^3 aliquot of 10 mmol dm^{-3} H_2PdCl_4 solution was added to 100 mL of 3.13 mmol dm^{-3} CTAB solution heated at 95˚C under stirring. After 5 min, 8 cm^3 of freshly prepared 10 mmol dm^{-3} ascorbic acid solution was added, and the reaction was allowed to proceed for 20 min. The obtained suspension was washed by ultra-pure water three times and the cubic Pd (c-Pd) suspension was prepared.

In the synthesis of octahedral Pd, a 4 cm^3 aliquot of 50 mmol dm^{-3} Na_2PdCl_4 solution was added to 7 cm^3 of an aqueous solution containing 116 mmol dm^{-3} of CTAC, 46 mmol dm^{-3} of citric acid and 50 mmol dm^{-3} of L-ascorbic acid heated at 95˚C under stirring[24-25]. The resultant solution was heated at 100˚C for 3 h with vigorous stirring. The obtained suspension was washed by ultra-pure water three times and the octahedral Pd (o-Pd) suspension was prepared.

2.2 Synthesis of metal hydroxide nanosheets

The metal hydroxide nanosheets were prepared thorough exfoliation of LDH precursors[26]. The LDH precursors were synthesized by the hydrothermal method[27-28]. For preparation of LDH-FeNi, $Ni(NO_3)_2 \cdot 6H_2O$ (Fujifilm Wako pure chemical corporation) and $Fe(NO_3)_3 \cdot 9H_2O$ (Kanto Chemical Co.) of which ratio of Ni to Fe was 3:1 were dissolved in 40 cm^3 of deionized water with 2 mmol of triethanolamine (TEA, Fujifilm Wako pure chemical corporation) to form a solution

with a total metal cation concentration of 80 mmol dm^{-3}. Then, 5.6 mmol of urea (Kanto Chemical Co.) were added to the solution and magnetically stirred for 1 h. Then, 40 cm^3 of the above solution was transferred to a 50 cm^3 stainless steel Teflon-lined autoclave and heated at 150˚C for 36 h. The obtained powder, LDH-FeNi, was collected by filtration and then washed with deionized water and ethanol. For preparation of LDH-MnNi, 0.5 mmol of $NiCl_2 \cdot 6H_2O$ (Fujifilm Wako pure chemical corporation) and 0.25 mmol of $MnCl_2 \cdot 4H_2O$ (Fujifilm Wako pure chemical corporation) were dissolved in 100 cm^3 of deionized water. 56.6 nm^3 of 30 wt% H_2O_2 (Fujifilm Wako pure chemical corporation), 1.5 mmol of NaCl (Fujifilm Wako pure chemical corporation) and 4.5 mmol of hexamethylenetetramine (HMT, Tokyo Chemical Industry Co., Ltd.) were added into the above solution. Then, the homogeneous solution was transferred into the autoclave and heated at 90°C for 4 h. A yellow product, LDH-MnNi, was collected by filtration and then washed with deionized water and ethanol.

Anion exchange was conducted in alcohol containing acid with an excess of the target anions [29]. An aqueous solution of perchlorate acid ($HClO_4$, 60%, Fujifilm Wako pure chemical corporation) was used for ClO_4^- anion exchange. The obtained LDH powders (100 mg) were dispersed into 100 cm^3 of Ar-purged methanol and mechanically stirred under Ar flow for 1 h. The obtained powders were collected by filtration and then washed with deionized water and ethanol. Finally, ClO_4^-–intercalated LDH powders were obtained after drying in vacuo at room temperature. For exfoliation, 5 mg of ClO_4^-–intercalated LDHs powders were dispersed in 10 cm^3 of degassed formamide and then mechanically stirred in a Ar atmosphere for 24 h. Transparent colloidal suspensions of FeNi and MnNi hydroxide nanosheets (FeNi-NS and MnNi-NS) were obtained.

2.3 Synthesis of composite catalysts

The colloidal suspensions of prepared Pd nanocrystals and nanosheets were mixed for several hours and then composite catalysts of Pd nanocrystals and metal hydroxide nanosheets were prepared. The nanosheets and Pd were combined in a 1:99 weight ratio. The composite catalysts are denoted as Pd/XNi, where X represents Fe or Mn.

2.3 Characterization

The phase of samples was examined by X-ray powder diffraction (XRD, Rigaku, Ultima IV) using Cu Kα radiation (λ = 0.15418 nm, U = 40 kV, I = 20 mA). Morphology of the prepared samples was observed using a low-voltage scanning electron microscope (SEM, Zeiss, Sigma-500) operated at 1.5 kV. The morphology and composition of the samples were also analyzed using a scanning transmission electron microscope (STEM, JEOL, JEM-ARM200F) with EDS facilities. The metal composition of catalysts was also determined by analyzing the solution of the samples dissolved in acid using the inductively coupled plasma atomic emission spectroscopy (ICP-AES, Shimadzu, ICPE-9000). The specimens of electrodes for cross-section observation were prepared using a cross-section polisher (JEOL, IB-19530CP).

2.4 Electrochemical measurement

The electrocatalytic activity was evaluated by the rotating disk electrode (RDE) system using the catalyst-loaded glassy carbon disk electrode. After polishing the glassy carbon disk electrode, 12 nm^3 of the colloidal suspensions of catalysts were dropped on the glassy carbon disk electrode,

and the solvent was evaporated at 90°C (loading of 8.15 μg cm^{-2}). The electrochemical measurements were carried out using a three-electrode system connected with VERTEX potentiostat/galvanostat (Ivium Technologies). A platinum coil and Hg/HgO/1 mol dm^{-3} KOH were used as counter and reference electrodes, respectively. All measurements were carried out at room temperature in 80 cm^3 of a 1 mol dm^{-3} KOH aqueous solution with and without 1 mol dm^{-3} ethanol (pH=14) under Ar atmosphere. The electrocatalytic activity was evaluated using cyclic voltammetry (CV). Before EOR, to remove the capping reagents which may bind to the facets of nanoparticles, electrochemical cleaning processes were performed before the EOR measurements. CV measurements were conducted in a 1 mol dm^{-3} KOH aqueous solution without 1 mol dm^{-3} ethanol as the blank condition with a potential sweep rate of 100 mV s^{-1}. Then, ethanol was added to the solution and CV measurements were carried out to evaluate the EOR activities. The potential was converted from the Hg/HgO/4 mol dm^{-3} KOH reference scale to the RHE using the following equation:

$$E \text{ vs RHE} = E \text{ vs Hg/HgO/4 mol dm}^{-3} \text{ KOH} + 0.926 \text{ V} \quad (1)$$

Chrono amperometry (CA) measurement was performed at 0.6 V vs RHE in an Ar-saturated 1 mol dm^{-3} KOH aqueous solution with 1 mol dm^{-3} ethanol solution. The CV curves were also measured from 0.0 to 1.2 V vs RHE to determine the electrochemically active surface area (ECSA) of Pd nanocrystals in the catalysts [10, 30-32]. The ECSA value was estimated according to the equation:

$$ECSA = Q/(0.405 \times W_{Pd}) \quad (2)$$

wherein Q represents the charge by integrating the reduction peak area of Pd oxide, W_{Pd} is the loading amount of Pd on the electrode, and the value of 0.405 mC cm^{-2} is the charge required for reduction of a Pd oxide single layer. Electric double layer capacitance (C_{dl}) was calculated to

estimate the ECSA of FeNi-NS and MnNi-NS by measuring the CV curves in the double layer capacitance region. The scan rates were 10, 20, 30, 40 and 50 mV s^{-1}. The C_{dl} was estimated by plotting the Δj (j_a-j_c) at 1.1 V vs RHE (1 mol dm^{-3} KOH) against the scan rate. The slope is twice of the C_{dl}.

Results and discussion

3.1 Morphology of LDH nanosheets

The LDH precursors were prepared using a hydrothermal method as reported previously [27-28]. After exchanging the carbonate anions in the LDH precursor for perchlorate anions, metal hydroxide nanosheets were exfoliated in formamide. TEM and SEM observations revealed that LDH precursors have typical plate-like morphologies with a lateral size of several hundred nanometers (Figure 1). The exfoliated nanosheets exhibited lateral sizes from several to several tens of nanometers with faint and uniform contrast. The results indicate that the nanosheets became a monolayer and fragment during exfoliation [14, 26]. The exfoliated nanosheets showed similar ECSA values (Figure S1). The EDX analysis indicated a nickel-iron ratio of 3:1 and a nickel-manganese ratio of 5:1 of each hydroxide nanosheets, which was similar to those of the corresponding LDH precursors. Therefore, we successfully prepared the monolayer metal hydroxide nanosheets with similar morphology, thickness, and different metal compositions.

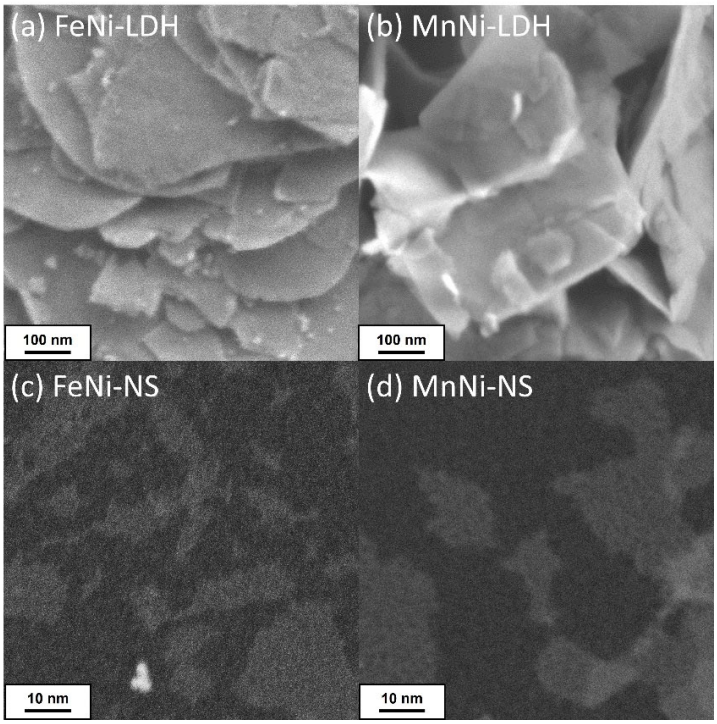

Figure 1 (a,b) SEM and (c,d) TEM images of FeNi- and MnNi-LDH precursors and NS.

3.2 Morphology of cubic and octahedral Pd nanoparticles

The cubic and octahedral Pd nanocrystals were prepared by one pot synthesis using shape-controlled reagents[19, 25]. Figure 2 shows the representative SEM and TEM images of the synthesized c- and o-Pd nanocrystals. Both Pd nanocrystals showed good uniformity in shape and narrow distribution in size with high selectivity (>95%). The mean sizes of diagonal line lie around 22 ± 2.1 and 22 ± 2.7 nm for the c- and o-Pd, respectively. The HRTEM images (Figure 2 (c) and (f)) revealed that the exposed surfaces of c-Pd and o-Pd are enclosed by (100) facets with d spacing 2.01 Å and (111) facets with d spacing 2.32 Å of the fcc Pd crystal, respectively. The corresponding SAED patterns (inset in Figure 2 (c) and (f)) also suggest the single crystal nature

of the obtained nanoparticles. The samples showed similar ECSA values obtained from CV as described later. Thus, we successfully synthesized well-faceted the cubic and octahedral Pd nanoparticles with the similar specific surface area.

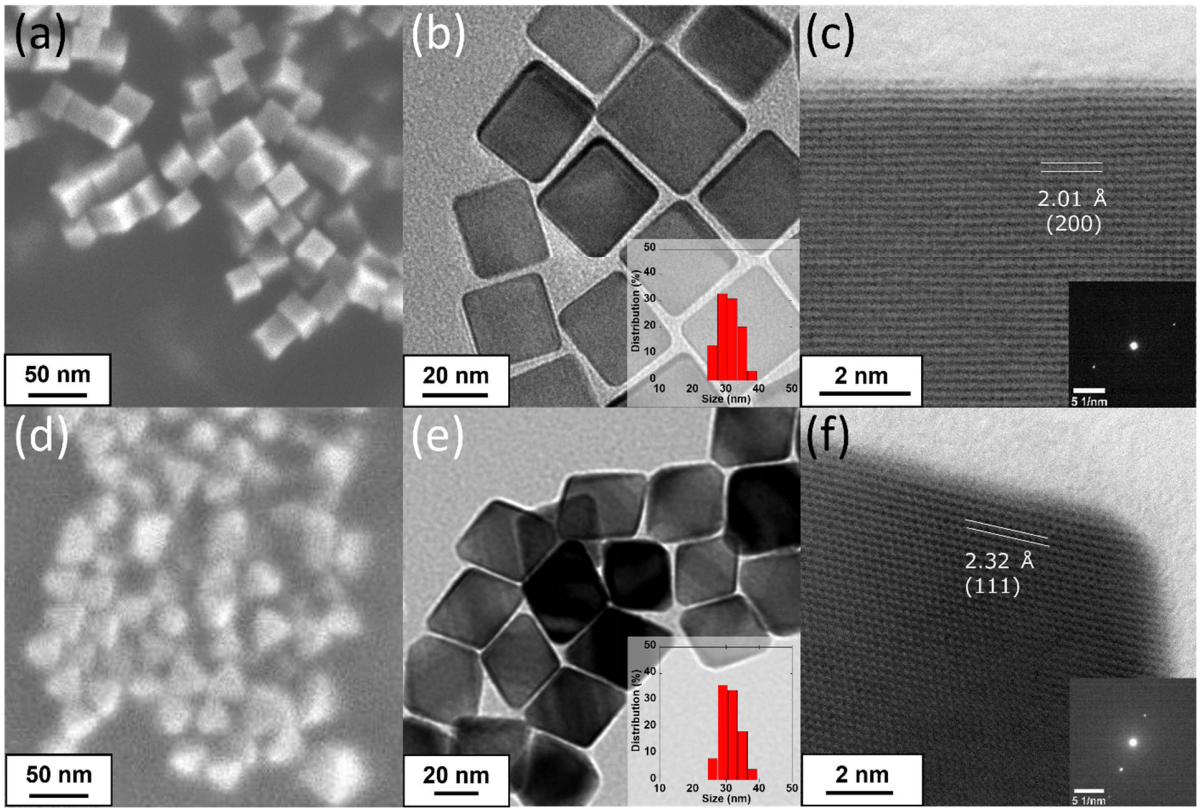

Figure 2 (a,d) SEM and (b,c,e,f) TEM images of (a-c) c- and (d-f) o-Pd nanocrystals. Insets in (b) and (e) show the particle size distributions and insets in (c) and (f) show the SAED patterns.

3.3 Morphology of composite catalysts

We investigated the morphology of composite catalysts and composite states at the interfaces between the faceted Pd surface and modifying nanosheets. Figure 3 shows high-angle annular dark-field STEM (HAADF-STEM) images of the composited catalysts. The all composite showed bright contrast of c- and o-Pd nanocrystals and faint contrast of hydroxide nanosheets with 2-3 nm thickness modified on the surface of Pd nanocrystals. The STEM-EDX mappings showed Pd signal overlapped with the Pd nanocrystals and Ni, Fe and Mn signals overlapped with the entire composite catalysts containing the nanosheets and Pd nanoparticles. This suggests that the hydroxide nanosheets were uniformly distributed on the surface of the Pd. High magnification STEM images clarified that metal hydroxide nanosheets were in contact with the Pd surface at their edges or lateral planes in all composite catalysts (Figure S2), showing that the fragmented fine nanosheets were modified on the (100) or (111) Pd facets in a random direction. Therefore, we successfully prepared the composite catalysts having similar interfacial states regardless of the Pd shape and metal composition of nanosheets.

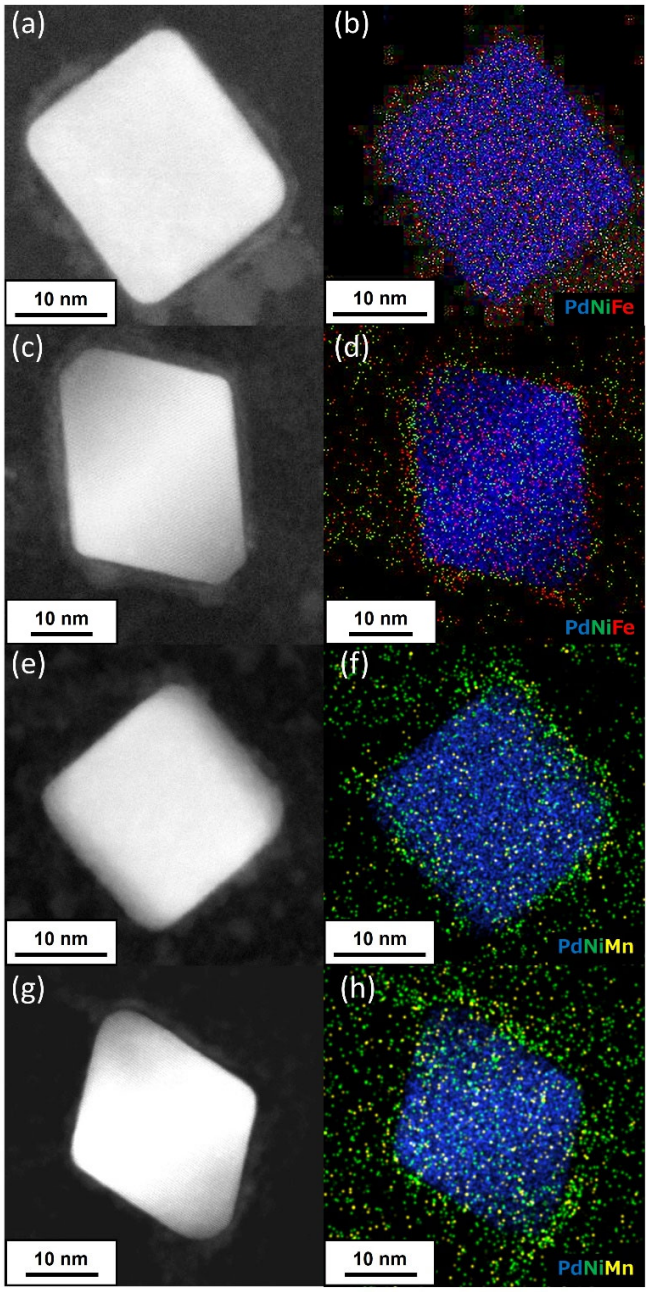

Figure 3 (a,c,e,g) HAADF-STEM images and (b,d,f,h) STEM-EDX mappings of (a,b) c-Pd/FeNi-NS, (c,d) o-Pd/FeNi-NS, (e,f) c-Pd/MnNi-NS and (g,h) o-Pd/MnNi-NS.

3.4 Valence states of the prepared catalysts

Since electronic states of catalysts intensively influence catalytic performances, we conducted XPS measurements to investigate the valence states of composed metals in the pristine samples and composite catalysts. Figure 4 shows XPS spectra of composed metals in the pristine Pd nanocrystals, hydroxide nanosheets and composite catalysts. Both the c- and o-Pd showed the Pd 3d spectra attributable to zero valent Pd, indicating that Pd surfaces have metallic states. The valence states of metals in the pristine nanosheets were assignable to Ni^{2+}, Fe^{3+}, Mn^{3+} and Mn^{4+}, similar to previous studies [14, 33]. Since the Mn species were easily oxidized in atmospheric conditions, Mn^{4+} species partially formed through oxidation of Mn^{3+}. For all the composite catalysts, XPS spectra of all metal elements were shifted to higher energy region compared to those for the corresponding pristine ones. The results were probably due to effects of the change in charge of the nanosheets through combination [11, 13, 15]. The metal hydroxide nanosheets inherently have a positive charge and intercalated anion species compensate the charge neutrality in the LDH stacks. The positive charge of exfoliated nanosheets in the suspensions was also compensated by the anions existing in neighboring circumstances. Because the exfoliated nanosheets in the composite catalysts were contacted on the Pd surfaces after combination with Pd nanoparticles, the anions could not sufficiently exist with the nanosheets for charge compensation and electrons were probably withdrawn from Pd nanocrystals. Thus, the valence states of Pd surface changed to more oxidative by nanosheet modification. Furthermore, previous studies reported that metal hydroxide such as $Ni(OH)_2$ converted to metal oxyhydroxide accompanied with oxidative change in valence states of metals [22, 34]. The results of the XPS analysis implied that metal hydroxide nanosheets were partially converted to metal oxyhydroxide. Thus, the electronic states of all metal species in the composite catalysts changed to the oxidative states compared to those of the

corresponding pristine samples. In comparing the electronic states of composite catalysts, the Pd 3d spectra for the Pd/MnNi-NS catalysts shifted to a higher energy region than those of Pd/FeNi-NS in both composite catalysts. Since the Mn ion can have higher valence states (Mn^{4+}) than that of the Fe ions (Fe^{3+}), the Pd surface states in the Pd/MnNi-NS composites changed to more oxidative than that in the Pd/FeNi-NS composites. Thus, the peak energy of Pd 3d in the catalyst was in the order of Pd/MnNi-NS > Pd/FeNi-NS > Pd. The composite catalysts showed similar energy shifts of Pd 3d spectra around 0.6 eV for Pd/FeNi-NS and 1.4 eV for the Pd/MnNi-NS regardless of Pd shape, respectively. The degree of change in electronic states of Pd by the combination of nanosheets was similar for the c-Pd and o-Pd.

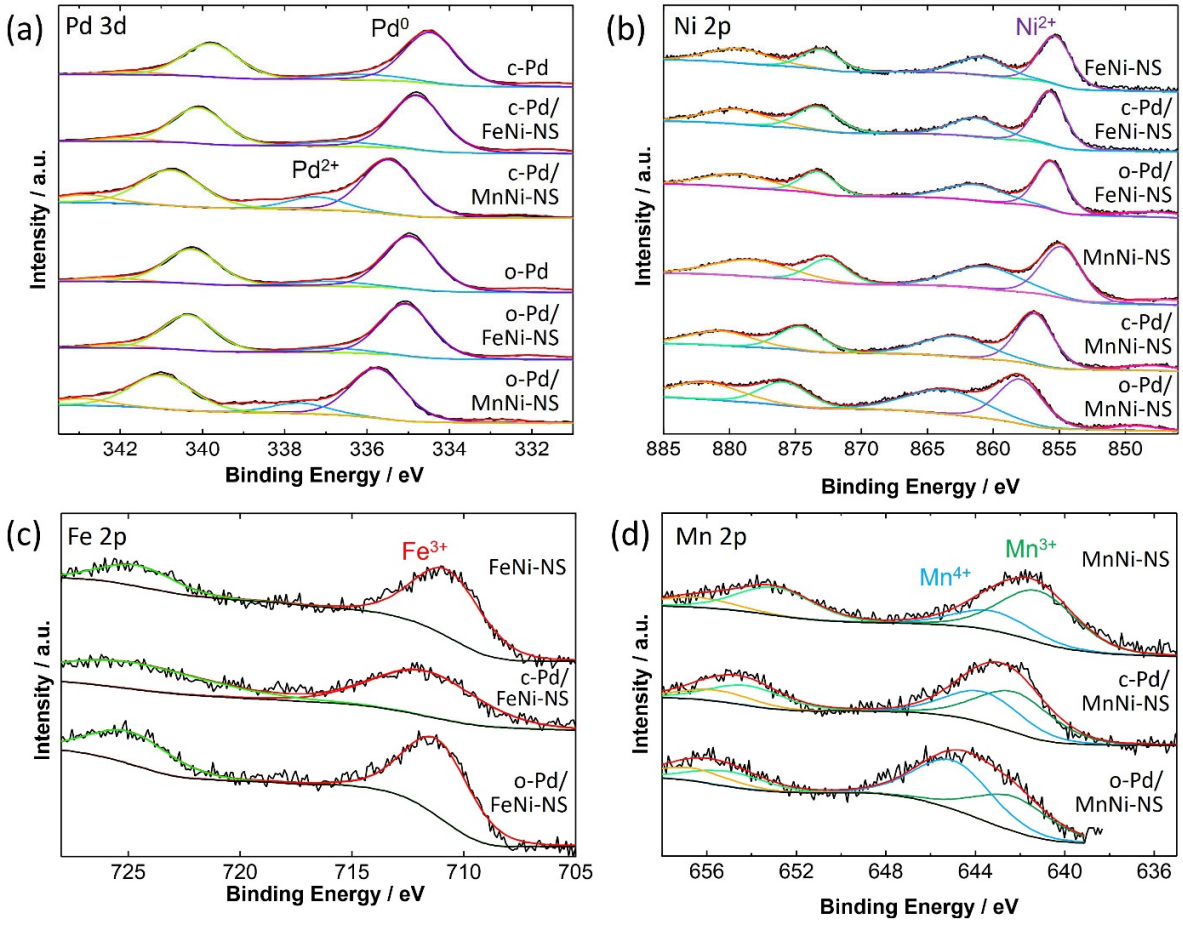

Figure 4 XPS spectra for (a) Pd 3d, (b) Ni 2p, (c) Fe 2p and (d) Mn 2p of pristine Pd nanocrystals, pristine NS and composite catalysts.

3.5 Catalytic performances of ethanol oxidation

The CV measurements were conducted to evaluate the electrochemical properties of the prepared samples in an Ar-saturated 1 mol dm^{-3} KOH aqueous solution at a potential sweep rate of 50 mV s^{-1} from 0 V to 1.2 V vs RHE (Figure 5 (a) and (b)). Current densities were normalized to the mass of Pd on the working electrode. All the CV curves exhibit a similar shape and several peaks can be clearly observed. Peaks from 0.1 to 0.3 V vs RHE were attributed to the hydrogen adsorption/desorption, while the cathodic peak from 0.6 to 0.9 V vs RHE corresponded to the reduction of Pd oxide to metallic Pd. The c-Pd and o-Pd showed similar ECSA, 0.043 and 0.040 m^2g^{-1}, respectively. The ECSA values of the c-Pd/FeNi-NS, c-Pd/MnNi-NS, o-Pd/FeNi-NS and c-Pd/MnNi-NS were determined to be 0.047, 0.043, 0.037 and 0.039 m^2g^{-1}, respectively, indicating no significant change in the ECSA of Pd after the combination of nanosheets.

The catalytic performances for EOR were evaluated by CV measurements in an Ar-saturated 1 mol dm^{-3} KOH aqueous solution with 1 mol dm^{-3} ethanol (Figure 5 (c) and (d)). All the catalysts showed an anodic peak in the forward scan between 0.5 and 0.9 V vs RHE, and an anodic peak in the reverse scan between 0.4 and 0.8 V. The former was typically assigned to the oxidation of ethanol to intermediate products, and the latter was attributed to the further oxidation of intermediate products, which is not completely oxidized during the forward scan [35-36]. Judging from the mass-specific current density in the forward scan, the c-Pd (2760 mA mg_{Pd}^{-1}) exhibited

a higher peak current for EOR than that of the o-Pd (2190 mA mg_{Pd}^{-1}). Since the bare samples showed a similar ECSA value, the activity difference was attributed to the catalytic properties of the (100) and (111) facet. Previous studies have reported that Pd catalysts with exposed (100) facet showed higher EOR activities than those with (111) facet [37-38], which is coincident with the present results. The catalytic activities of composite catalysts were compared with those of bare Pd catalysts under the same condition. The composite catalysts showed higher activities than corresponding bare Pd for each shape, i.e., the peak current of c-Pd/FeNi-NS (3040 mA mg_{Pd}^{-1}) and c-Pd/MnNi-NS (3140 mA mg_{Pd}^{-1}) is higher than that of c-Pd, and that of o-Pd/FeNi-NS (2680 mA mg_{Pd}^{-1}) and o-Pd/MnNi-NS (3140 mA mg_{Pd}^{-1}) is higher than that of o-Pd. Since the hydroxide nanosheets alone did not show EOR activities, Pd is an active site for EOR in the composite catalyst and the combination of nanosheets clearly improved EOR activities of the Pd crystals. The EOR performances of composite catalysts depended on the metal composition of nanosheets and the Pd/MnNi-NS showed higher EOR performances than those of the Pd/FeNi-NS in each Pd shape.

The CA measurements were performed to assess the durability of catalysts at 0.6 V vs RHE in alkaline media (Figure 5 (e)). For all electrocatalysts, the mass-specific current densities rapidly decreased at the initial reaction stage and then declined with the prolongation of time. Similar behaviors have been frequently observed in previous studies [39-41]. The sharp drop in current density is attributed to the formation of carbonaceous intermediates on the surface of catalysts during the EOR, which block the active sites and decrease the electrochemical activities. The c-Pd showed higher initial current density than that of o-Pd; however, both pristine Pd showed a rapid decrease in current density and no activity within 200 s due to the poisoning of carbonous intermediates. The composite electrocatalysts showed a higher current density than those of the corresponding

pristine Pd, which was similar to the CV results. Furthermore, the composite catalysts exhibited slower activity decay than the pristine Pd, suggesting the promotion of poisoning tolerance by combining nanosheets. Thus, the combination of nanosheets with Pd enhanced not only activities but also durability for EOR. The CA performances of composite catalysts also depended on nanosheet metal composition, and the Pd/MnNi-NS showed higher performances than those of the Pd/FeNi-NS for each Pd morphology.

Previous studies have suggested that a possible reason for the activity enhancement by the hydroxide modification on metal nanoparticles is the change in the electronic states of active sites [11, 13, 15]. The valence states of Pd changed oxidatively by nanosheet modification, and Pd in the Pd/MnNi-NS showed more oxidative states than that in the Pd/FeNi-NS. The order of peak current in the CV and current density in the CA of the catalysts for each Pd shape is consistent with the order of peak energy of Pd 3d in XPS, i.e., Pd/MnNi-NS > Pd/FeNi-NS > Pd. Therefore, the results indicate that electronic states of Pd significantly contribute to the EOR activities and the catalysts with more oxidative states of Pd show higher EOR activities.

Comparing the Pd shape, the c-Pd/NiMn-NS and c-Pd/NiFe-NS exhibited peak current about 1.1 and 1.05 times higher than that of the c-Pd alone, respectively, while the o-Pd/NiMn-NS and o-Pd/NiFe-NS exhibited the peak current about 1.5 and 1.3 times higher than that of the o-Pd alone in the CV measurements. Furthermore, o-Pd/MnNi-NS showed similar or slightly higher performances than those of c-Pd/MnNi-NS, that is, lower overpotential on the CV and slower current density decay on the CA while the o-Pd and o-Pd/FeNi-NS catalysts exhibited lower activities than those of the corresponding c-Pd catalysts. The results indicate that the degree of activity enhancement by nanosheet modification was greater for o-Pd than for c-Pd. Even though similar changes in valence states of Pd due to combination with FeNi-NS and MnNi-NS were

observed from XPS regardless the Pd shape, the variation of activity enhancement suggests that another factor derived from the combination also contributed to activity enhancement in the composite catalysts. The difference in activity enhancement would be due to the effects of nanosheet modification on each facet. We discuss mechanisms of activity enhancement in the composite catalysts in the next section.

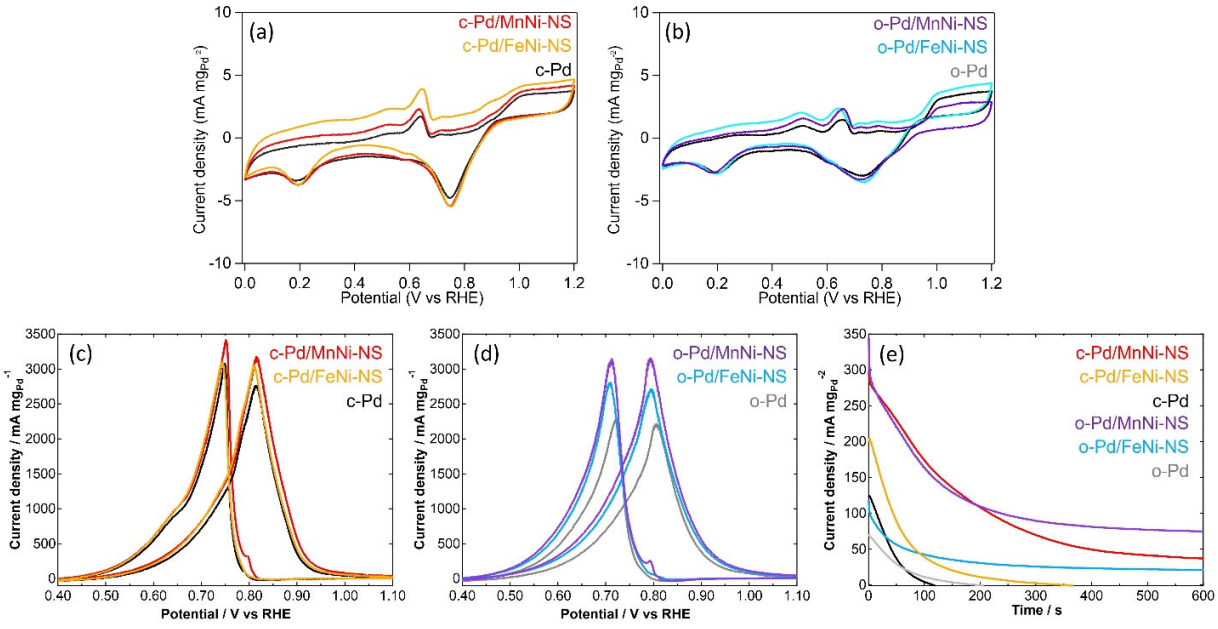

Figure 5 Electrochemical measurements of prepared catalysts. (a, b) CV curves of the pristine Pd nanocrystals and composite catalysts at 100 mV s^{-1} under the blank condition. (c, d) CV curves of the pristine Pd nanocrystals and composite catalysts at 100 mV s^{-1} in an Ar-saturated 1 mol dm^{-3} KOH aqueous solution with 1 mol dm^{-3} ethanol. (e) Long-time durability of the pristine Pd nanocrystals and composite catalysts at 0.6 V vs RHE.

3.6 Mechanism of catalytic performance improvement

Since the adsorption energy of substrates and intermediates affects the activation energy of elementary steps in electrochemical reactions, the electronic states of the catalyst, which influences their adsorption energy, are regarded as important factors [42-43]. Previous studies reported that catalytic activities of many composite catalysts were enhanced by a change in the electronic states of active sites due to electron transfer between component materials [44-46]. In this study, the electronic states of Pd oxidatively changed by combination with nanosheets and the oxidative change in electronic states probably increased the adsorption energy of ethanol and intermediates, promoting the EOR. The higher EOR performances of Pd/MnNi-NS than those of Pd/FeNi-NS were attributed to stronger ethanol adsorption on the Pd.

In addition to the electronic states of Pd, OH^- adsorption also influenced on the EOR performances in the composite catalysts [9-10, 15, 30]. In Pd nanocrystals, experimental and computational studies have pointed out that octahedral Pd with (111) facet is less active than cubic Pd with (100) facet [37-38, 47-48], and have proposed that the low activity of the (111) facet was mainly due to the low adsorption energy of OH^- rather than the low adsorption energy of ethanol or intermediates on the surface[37, 49-50]. For alkaline EOR, adsorbed OH^- species assist dehydrogenation of ethanol and oxidative removal of intermediates. The (111) surface is less favorable than the (100) surface for EOR since adsorption energy of OH^- on (111) facet is lower than that on (100) facet. In composite catalysts of Pd nanoparticles and metal hydroxides, OH^- is easily adsorbed on the metal ion centers of the hydroxide due to their higher affinity to oxygen than that of Pd. Since the OH^- species adsorbed on metal hydroxides promote the dehydrogenation of ethanol and the oxidation reaction of intermediates at interfacial sites between Pd nanoparticles and metal hydroxides, composite catalysts achieved higher EOR performances than those of bare Pd catalysts in previous studies[9-

[10, 15, 30]. For the composite catalysts in this study, OH^- species adsorbed on nanosheets could promote the EOR performances under a similar process. However, the degree of activity enhancement due to the promotion of OH^- adsorption by nanosheets differed for the (100) and (111) facets. Catalytic activities of the o-Pd with (111) facet were lower than those of the c-Pd with (100) facet mainly due to the energetically unfavorable adsorption of OH for Pd alone. The promotion of OH^- adsorption by nanosheets reduced the difference in activities on the facets in the composite catalysts. Thus, the degree of activity enhancement by nanosheet modification was relatively greater for o-Pd than for c-Pd.

The o-Pd/MnNi-NS partially showed higher EOR performances than those of c-Pd/MnNi-NS, such as the overpotential in the CV and current density decay in the CA. Ensemble effects may occur when ethanol molecules adsorbed on a particular crystal facet react with OH^- on the hydroxide rather than OH- adsorbed on Pd. A computational study will elucidate the activity trends of the composite catalysts, which would be the next challenge. In this study, we applied relatively large Pd nanocrystals with around 20 nm to clearly elucidate the effects of the facets on the EOR performances of the composite catalysts. Excellent activities will be achieved by the combination of fine Pd nanocrystals with several nanometers and porous metal hydroxide supporting the Pd nanocrystals with high dispersion. Based on the results, the combination of metal hydroxide nanosheets and the Pd (111) facet, which induces the oxidative valence states of Pd and promotes OH^- adsorption, is the promising approach to develop highly active electrocatalysts for EOR.

Conclusion

We synthesized composite electrocatalysts of the c-Pd with (100) facet and o-Pd with (111) facet with FeNi-NS and MnNi-NS for EOR and systematically investigated the combination effects of metal hydroxide on the Pd facets on the EOR performances. The valence states of Pd were oxidatively changed by nanosheets modification and the Pd in the Pd/MnNi composites had more oxidative state than that in the Pd/FeNi-NS composites for both shapes due to high valence states of Mn^{4+}. Modification of nanosheets improved catalytic performances of Pd for EOR and the composite catalysts with higher oxidative states showed higher EOR activities due to stronger adsorption of ethanol and intermediates. Although the c-Pd was superior for EOR than the o-Pd in the bare Pd nanocrystals, the degree of activity enhancement by nanosheet modification was greater for o-Pd than for c-Pd due to the effects of promotion of OH^- adsorption and the o-Pd/MnNi-NS showed the highest EOR performances. The results suggests that the combination of metal hydroxides and the Pd (111) facet provides promising catalyst designs to develop highly active electrocatalysts for EOR.

AUTHOR INFORMATION

Corresponding Author

*Sho Kitano

E-mail: skitano@eng.hokudai.ac.jp

Phone: +81-92-802-6735.

*Hiroki Habazaki

E-mail: habazaki@eng.hokudai.ac.jp

Phone: +81-92-802-6874.

Author Contributions

S. Kitano; Conceptualization, Supervision, Visualization, Resources, Writing- Review & Editing, Funding acquisition, Methodology.: H. Motohashi; Investigation, Data curation, Methodology.: M. Iwai; Investigation, Methodology.: K. Fushimi; Investigation, Methodology.: Y. Aoki; Investigation, Methodology.: H. Habazaki; Conceptualization, Supervision, Visualization, Resources, Writing- Review & Editing, Funding acquisition, Methodology. All authors have given approval to the final version of the manuscript.

Funding Sources

Part of this study was conducted at the Laboratory of XPS analysis, Joint-use facilities and the Multi-Quantum Beam High Voltage Electron Microscope Laboratory at Hokkaido University, supported by the Nanotechnology Platform Program of the Ministry of Education, Culture, Sports, Science and Technology (MEXT), Japan (A-21-HK-0035). We acknowledge funding by JSPS KAKENHI (22K05295), Japan.

REFERENCES

1. Ong, B. C.; Kamarudin, S. K.; Basri, S., Direct liquid fuel cells: A review. *Int J Hydrogen Energ* **2017,** *42* (15), 10142-10157.

2. Kamarudin, M. Z. F.; Kamarudin, S. K.; Masdar, M. S.; Daud, W. R. W., Review: Direct ethanol fuel cells. *Int J Hydrogen Energ* **2013,** *38* (22), 9438-9453.
3. Akhairi, M. A. F.; Kamarudin, S. K., Catalysts in direct ethanol fuel cell (DEFC): An overview. *Int J Hydrogen Energ* **2016,** *41* (7), 4214-4228.
4. Wang, Y. R.; He, Q. L.; Guo, J.; Wang, J. M.; Luo, Z. P.; Shen, T. D.; Ding, K. Q.; Khasanov, A.; Wei, S. Y.; Guo, Z. H., Ultrafine FePd Nanoalloys Decorated Multiwalled Cabon Nanotubes toward Enhanced Ethanol Oxidation Reaction. *Acs Appl Mater Inter* **2015,** *7* (43), 23920-23931.
5. Friedl, J.; Stimming, U., Model catalyst studies on hydrogen and ethanol oxidation for fuel cells. *Electrochim Acta* **2013,** *101*, 41-58.
6. Zhang, L. L.; Chang, Q. W.; Chen, H. M.; Shao, M. H., Recent advances in palladium-based electrocatalysts for fuel cell reactions and hydrogen evolution reaction. *Nano Energy* **2016,** *29*, 198-219.
7. Chen, A. C.; Ostrom, C., Palladium-Based Nanomaterials: Synthesis and Electrochemical Applications. *Chem Rev* **2015,** *115* (21), 11999-12044.
8. Antolini, E., Palladium in fuel cell catalysis. *Energ Environ Sci* **2009,** *2* (9), 915-931.
9. Li, C.; Wen, H.; Tang, P. P.; Wen, X. P.; Wu, L. S.; Dai, H. B.; Wang, P., Effects of Ni(OH) Morphology on the Catalytic Performance of Pd/Ni(OH)/Ni Foam Hybrid Catalyst toward Ethanol Electrooxidation. *Acs Appl Energ Mater* **2018,** *1* (11), 6040-6046.

10. Huang, W. J.; Ma, X. Y.; Wang, H.; Feng, R. F.; Zhou, J. G.; Duchesne, P. N.; Zhang, P.; Chen, F. J.; Han, N.; Zhao, F. P.; Zhou, J. H.; Cai, W. B.; Li, Y. G., Promoting Effect of Ni(OH) on Palladium Nanocrystals Leads to Greatly Improved Operation Durability for Electrocatalytic Ethanol Oxidation in Alkaline Solution. *Adv Mater* **2017,** *29* (37).

11. Chen, Z. L.; Liu, Y. W.; Liu, C.; Zhang, J. F.; Chen, Y. N.; Hu, W. B.; Deng, Y. D., Engineering the Metal/Oxide Interface of Pd Nanowire@CuO

Electrocatalysts for Efficient Alcohol Oxidation Reaction. *Small* **2020,** *16* (4).
12. Niu, M. Y.; Xu, W. C.; Zhu, S. L.; Liang, Y. Q.; Cui, Z. D.; Yang, X. J.; Inoue, A., Synthesis of nanoporous CuO/TiO/Pd-NiO composite catalysts by chemical dealloying and their performance for methanol and ethanol electro-oxidation. *J Power Sources* **2017,** *362*, 10-19.

13. Liu, F. L.; Gao, X. T.; Shi, R.; Guo, Z. X.; Tse, E. C. M.; Chen, Y., Concerted and Selective Electrooxidation of Polyethylene-Terephthalate-Derived Alcohol to Glycolic Acid at an Industry-Level Current Density over a Pd-Ni(OH) Catalyst. *Angew Chem Int Edit* **2023,** *62* (11).

14. Kitano, S.; Noguchi, T. G.; Nishihara, M.; Kamitani, K.; Sugiyama, T.; Yoshioka, S.; Miwa, T.; Yoshizawa, K.; Staykov, A.; Yamauchi, M., Heterointerface Created on Au-Cluster-Loaded Unilamellar Hydroxide Electrocatalysts as a Highly Active Site for the Oxygen Evolution Reaction. *Adv Mater* **2022,** *34* (16).
15. Yuan, X. L.; Zhang, Y.; Cao, M. H.; Zhou, T.; Jiang, X. J.; Chen, J. X.; Lyu, F. L.; Xu, Y.; Luo, J.; Zhang, Q.; Yin, Y. D., Bi(OH)/PdBi Composite Nanochains as Highly Active and Durable Electrocatalysts for Ethanol Oxidation. *Nano Lett* **2019,** *19* (7), 4752-4759.

16. Shi, Y. F.; Lyu, Z. H.; Zhao, M.; Chen, R. H.; Nguyen, Q. N.; Xia, Y. N., Noble-Metal Nanocrystals with Controlled Shapes for Catalytic and Electrocatalytic Applications. *Chem Rev* **2021,** *121* (2), 649-735.
17. Rizo, R.; Roldan Cuenya, B., Shape-Controlled Nanoparticles as Anodic Catalysts in Low-Temperature Fuel Cells. *Acs Energy Lett* **2019,** *4* (6), 1484-1495.
18. Choi, S. I.; Herron, J. A.; Scaranto, J.; Huang, H. W.; Wang, Y.; Xia, X. H.; Lv, T.; Park, J. H.; Peng, H. C.; Mavrikakis, M.; Xia, Y. N., A Comprehensive Study of Formic Acid Oxidation on Palladium Nanocrystals with Different Types of Facets and Twin Defects. *Chemcatchem* **2015,** *7* (14), 2077-2084.
19. Niu, W. X.; Zhang, L.; Xu, G. B., Shape-Controlled Synthesis of Single-Crystalline Palladium Nanocrystals. *Acs Nano* **2010,** *4* (4), 1987-1996.
20. Jin, M. S.; Zhang, H.; Xie, Z. X.; Xia, Y. N., Palladium nanocrystals enclosed by {100} and {111} facets in controlled proportions and their catalytic activities for formic acid oxidation. *Energ Environ Sci* **2012,** *5* (4), 6352-6357.
21. Iqbal, M.; Kaneti, Y. V.; Kim, J.; Yuliarto, B.; Kang, Y. M.; Bando, Y.; Sugahara, Y.; Yamauchi, Y., Chemical Design of Palladium-Based Nanoarchitectures for Catalytic Applications. *Small* **2019,** *15* (6).
22. Zhou, D. J.; Li, P. S.; Lin, X.; McKinley, A.; Kuang, Y.; Liu, W.; Lin, W. F.; Sun, X. M.; Duan, X., Layered double hydroxide-based electrocatalysts for the oxygen evolution reaction: identification and tailoring of active sites, and superaerophobic nanoarray electrode assembly. *Chem Soc Rev* **2021,** *50* (15), 8790-8817.
23. Fan, G. L.; Li, F.; Evans, D. G.; Duan, X., Catalytic applications of layered double hydroxides: recent advances and perspectives. *Chem Soc Rev* **2014,** *43* (20), 7040-7066.
24. Hong, J. W.; Kim, D.; Lee, Y. W.; Kim, M.; Kang, S. W.; Han, S. W., Atomic-Distribution-Dependent Electrocatalytic Activity of Au-Pd Bimetallic Nanocrystals. *Angew Chem Int Edit* **2011,** *50* (38), 8876-8880.
25. Lee, Y. W.; Kim, M.; Kim, Z. H.; Han, S. W., One-Step Synthesis of Au@Pd Core-Shell Nanooctahedron. *J Am Chem Soc* **2009,** *131* (47), 17036-+.
26. Song, F.; Hu, X. L., Exfoliation of layered double hydroxides for enhanced oxygen evolution catalysis. *Nat Commun* **2014,** *5*.
27. Ma, W.; Ma, R. Z.; Wu, J. H.; Sun, P. Z.; Liu, X. H.; Zhou, K. C.; Sasaki, T., Development of efficient electrocatalysts molecular hybridization of NiMn layered double hydroxide nanosheets and graphene. *Nanoscale* **2016,** *8* (19), 10425-10432.

28. Abellán, G.; Coronado, E.; Martí-Gastaldo, C.; Pinilla-Cienfuegos, E.; Ribera, A., Hexagonal nanosheets from the exfoliation of Ni-Fe LDHs: a route towards layered multifunctional materials. *J Mater Chem* **2010,** *20* (35), 7451-7455.

29. Iyi, N.; Yamada, H.; Sasaki, T., Deintercalation of carbonate ions from carbonate-type layered double hydroxides (LDHs) using acid-alcohol mixed solutions. *Appl Clay Sci* **2011,** *54* (2), 132-137.
30. Yang, H.; Zhang, A.; Bai, Y.; Chu, M.; Li, H.; Liu, Y.; Zhu, P.; Chen, X.; Deng, C. W.; Yuan, X. L., One Stone Two Birds: Unlocking the Synergy between Amorphous Ni(OH) and Pd Nanocrystals toward Ethanol and Formic Acid Oxidation. *Inorg Chem* **2022,** *61* (36), 14419-14427.

31. Du, W. X.; Mackenzie, K. E.; Milano, D. F.; Deskins, N. A.; Su, D.; Teng, X. W., Palladium-Tin Alloyed Catalysts for the Ethanol Oxidation Reaction in an Alkaline Medium. *Acs Catal* **2012,** *2* (2), 287-297.
32. Xiao, L.; Zhuang, L.; Liu, Y.; Lu, J. T.; Abruña, H. D., Activating Pd by Morphology Tailoring for Oxygen Reduction. *J Am Chem Soc* **2009,** *131* (2), 602-608.
33. Hong, J. D.; Chen, C. P.; Siriviriyanun, A.; Crivoi, D. G.; Holdway, P.; Buffet, J. C.; O'Hare, D., NiMn-layered double oxide electrodes in organic electrolyte based supercapacitors. *Rsc Adv* **2021,** *11* (44), 27267-27275.

34. Trafela, S.; Zavasnik, J.; Sturm, S.; Rozman, K. Z., Formation of a Ni(OH)/NiOOH active redox couple on nickel nanowires for formaldehyde detection in alkaline media. *Electrochim Acta* **2019,** *309*, 346-353.

35. Chen, A. C.; Holt-Hindle, P., Platinum-Based Nanostructured Materials: Synthesis, Properties, and Applications. *Chem Rev* **2010,** *110* (6), 3767-3804.
36. Xu, C. W.; Wang, H.; Shen, P. K.; Jiang, S. P., Highly ordered Pd nanowire arrays as effective electrocatalysts for ethanol oxidation in direct alcohol fuel cells. *Adv Mater* **2007,** *19* (23), 4256-+.
37. Ma, X. Y.; Chen, Y. F.; Wang, H.; Li, Q. X.; Lin, W. F.; Cai, W. B., Electrocatalytic oxidation of ethanol and ethylene glycol on cubic, octahedral and rhombic dodecahedral palladium nanocrystals. *Chem Commun* **2018,** *54* (20), 2562-2565.
38. Qi, K.; Wang, Q. Y.; Zheng, W. T.; Zhang, W.; Cui, X. Q., Porous single-crystalline palladium nanoflowers with enriched {100} facets for highly enhanced ethanol oxidation. *Nanoscale* **2014,** *6* (24), 15090-15097.
39. Sulaiman, J. E.; Zhu, S. Q.; Xiang, Z. L.; Chang, Q. W.; Shao, M. H., Pt-Ni Octahedra as Electrocatalysts for the Ethanol Electro-Oxidation Reaction. *Acs Catal* **2017,** *7* (8), 5134-5141.
40. Chen, L.; Lu, L. L.; Zhu, H. L.; Chen, Y. G.; Huang, Y.; Li, Y. D.; Wang, L. Y., Improved ethanol electrooxidation performance by shortening Pd-Ni active site distance in Pd-Ni-P nanocatalysts. *Nat Commun* **2017,** *8*.
41. Cai, B.; Wen, D.; Liu, W.; Herrmann, A. K.; Benad, A.; Eychmüller, A., Function-Led Design of Aerogels: Self-Assembly of Alloyed PdNi Hollow Nanospheres for Efficient Electrocatalysis. *Angew Chem Int Edit* **2015,** *54* (44), 13101-13105.
42. Wang, Y. W.; Qiu, W. J.; Song, E. H.; Gu, F.; Zheng, Z. H.; Zhao, X. L.; Zhao, Y. Q.; Liu, J. J.; Zhang, W. Q., Adsorption-energy-based activity descriptors for electrocatalysts in energy storage applications. *Natl Sci Rev* **2018,** *5* (3), 327-341.
43. Seh, Z. W.; Kibsgaard, J.; Dickens, C. F.; Chorkendorff, I. B.; Norskov, J. K.; Jaramillo, T. F., Combining theory and experiment in electrocatalysis: Insights into materials design. *Science* **2017,** *355* (6321).
44. Lyu, F. L.; Cao, M. H.; Mahsud, A.; Zhang, Q., Interfacial engineering of noble metals for electrocatalytic methanol and ethanol oxidation. *J Mater Chem A* **2020,** *8* (31), 15445-15457.
45. Xiang, R.; Peng, L. S.; Wei, Z. D., Tuning Interfacial Structures for Better Catalysis of Water Electrolysis. *Chem-Eur J* **2019,** *25* (42), 9799-9815.
46. Shao, Q.; Wang, P. T.; Huang, X. Q., Opportunities and Challenges of Interface Engineering in Bimetallic Nanostructure for Enhanced Electrocatalysis. *Adv Funct Mater* **2019,** *29* (3).
47. Monyoncho, E. A.; Steinmann, S. N.; Michel, C.; Baranova, E. A.; Woo, T. K.; Sautet, P., Ethanol Electro-oxidation on Palladium Revisited Using Polarization Modulation Infrared

Reflection Absorption Spectroscopy (PM-IRRAS) and Density Functional Theory (DFT): Why Is It Difficult To Break the C-C Bond? *Acs Catal* **2016,** *6* (8), 4894-4906.
48. Wang, E. D.; Xu, J. B.; Zhao, T. S., Density Functional Theory Studies of the Structure Sensitivity of Ethanol Oxidation on Palladium Surfaces. *J Phys Chem C* **2010,** *114* (23), 10489-10497.
49. Guo, Y. G.; Li, B. Y.; Shen, S. Y.; Luo, L. X.; Wang, G. F.; Zhang, J. L., Potential-Dependent Mechanistic Study of Ethanol Electro-oxidation on Palladium. *Acs Appl Mater Inter* **2021,** *13* (14), 16602-16610.
50. Sheng, T.; Lin, W. F.; Hardacre, C.; Hu, P., Role of Water and Adsorbed Hydroxyls on Ethanol Electrochemistry on Pd: New Mechanism, Active Centers, and Energetics for Direct Ethanol Fuel Cell Running in Alkaline Medium. *J Phys Chem C* **2014,** *118* (11), 5762-5772.